Journal of Oceanology and Limnology
Vol. 42, No. 2, pp. 492-510, 2024
https://doi.org/10.1007/s00343-023-2350-z

Research Paper

Persistent mixing bursts in the equatorial Pacific thermocline induced by persistent equatorial waves*

Jingjing ZHANG[1, 2], Chuanyu LIU[2, 3, **], Xiang GONG[1], Fan WANG[2, 3]

[1] *School of Mathematics and Physics, Qingdao University of Science and Technology, Qingdao 266100, China*

[2] *Key Laboratory of Ocean Circulation and Waves, Institute of Oceanology, Chinese Academy of Sciences, Qingdao 266071, China*

[3] *Laoshan Laboratory, Qingdao 266237, China*

Received Oct. 24, 2022; accepted in principle Dec. 28, 2022; accepted for publication May 5, 2023

Abstract A recent study by Liu et al. (2020) suggested that due to the saturation of equatorially trapped planetary waves with different dynamical types, temporal periods, meridional and baroclinic modes, complex layer structures of vertical velocity shear and hence turbulent mixing could frequently occur in the thermocline of the eastern equatorial Pacific. We investigated the occurrence of the interior turbulent mixing as indicated by shear instabilities, above the Equatorial Undercurrent (EUC) core at three equatorial sites along 140°W, 170°W, and 165°E, respectively, based mainly on data from the Tropical Atmosphere and Ocean (TAO) mooring array. We found that turbulent mixing bursts persisted in the thermocline of all three sites. Specifically, the interior turbulent mixing layers (ITMLs) could occur in probability of approximately 68%, 53%, and 48% at the three sites, respectively. The overall occurrence probability shows obvious and similar biannual variations at 140°W and 170°W, which is higher in boreal from late summer to winter and lower in spring. Vertically, the ITMLs are primarily located above the EUC core and prevail in deeper (shallower) layers from late summer to winter (spring). Most ITMLs (70%) lasted for hours to 3 days, and a few of them (15%) for more than 7 days. The thicknesses of ITMLs were concentrated between 15 and 55 m. At 165°E, the vertical distribution of ITML occurrence probability was different from that at 140°W and 170°W, as it did not show a preference for depths; the durations of ITMLs are short (also from hours to several days) and their thicknesses were between 5 and 25 m. These properties, particularly the high occurrence probability, and short durations demonstrated the persistence of thermocline mixing in the western to eastern equatorial Pacific thermocline and confirmed the generation mechanism by persistent equatorial waves as well.

Keyword: interior turbulent mixing layer (ITML); weakly sheared layer (WSL); Equatorial Undercurrent (EUC) core; occurrence probability; seasonality

1 INTRODUCTION

The surface mixed layer (ML) in the equatorial cold tongue of the central and eastern Pacific plays an important role in tropical atmosphere-ocean interactions. The thermal structure of the ML is governed by the balance of cooling due to the vertical turbulent heat flux at the base of the ML (~100 W/m^2), warming by the net heat fluxes from the surface (~70 W/m^2), and horizontal heat advection (~50 W/m^2) (Wang and McPhaden, 1999, 2001). Additionally, direct turbulence observations have demonstrated that the seasonal variation of sea surface temperature (SST) is controlled by the subsurface turbulent heat flux (Moum et al., 2013). It has also been indicated that the subsurface turbulent heat flux exerts positive feedback on the phase change of the El Niño and Southern

* Supported by the National Natural Science Foundation of China (NSFC) (No. 41730534), the Laoshan Laboratory Science and Technology Innovation Program (No. LSKJ202202502), the NSFC (Nos. 41976012, 42090044), and the Strategic Priority Research Program of Chinese Academy of Sciences (No. XDB42000000)

** Corresponding author: chuanyu.liu@qdio.ac.cn

Oscillation (ENSO) (Warner and Moum, 2019). Numerical models have suggested that smaller (bigger) background vertical diffusivity in the thermocline may lead to a larger (smaller) amplitude of El Niño (Meehl et al., 2001). Therefore, much research focused on the dynamics of turbulence within the ML and their representation in numerical models.

Turbulence has been intensively observed in the upper flank of the thermocline at 0°, 140°W (referred to as Eq140°W hereafter) by several expeditions, including Tropic Heat 1 (TH1, 1984; Gregg et al., 1985; Moum and Caldwell, 1985), Tropic Heat 2 (TH2, 1987; Peters et al., 1991), the Tropical Instability Wave Experiment (TIWE, 1991; Lien et al., 1995), and the Equatorial Internal Wave Experiment (EQUIX, 2008; Moum et al., 2009; Inoue et al., 2012). These measurements have revealed unique turbulent processes that determine the heat transport from the ML to the thermocline. In particular, TH1 revealed a deep-cycle layer (DCL) of turbulence penetrating the upper thermocline. The nighttime turbulent kinetic energy dissipation rate in the DCL exceeded the daytime value by more than an order of magnitude (Moum et al., 1992, 2011). Subsequent studies have shown that the DCL is an omnipresent feature at Eq140°W. EQUIX revealed an unusual layer of elevated shear and turbulence immediately above the core of the Equatorial Undercurrent (EUC), which was named the upper core layer (UCL). The UCL was about 50 m thick and with highly elevated turbulence. During different phases of the passage of an equatorial mode of the tropical instability wave (TIW) (Liu et al., 2019b), the UCL appeared to be merged with the surface-driven DCL (at 50–100-m depth) or dynamically separated from the DCL by thin, weakly sheared, essentially non-turbulent (laminar) layers (referred to as WSLs hereafter; Moum et al., 2009; Inoue et al., 2012). A prominent WSL was centered at ~50-m depth, was about 25 m thick, and occurred during November 4–7, 2008, while another WSL was found at ~50–80 m on November 1–2, 2008.

The diurnal turbulent DCL was considered to be initiated by surface momentum and buoyancy forcings, as referenced in Inoue et al. (2012). On the other hand, the turbulent UCL was shown to be generated by the interplay among a set of multiple-temporal-scale equatorial waves with the mean equatorial currents, as demonstrated by Liu et al. (2020) and related work (Liu et al., 2019a, b; Natarov and Richards, 2019). Generally, two mechanisms were found to be critical for the generation of the turbulent UCL and non-turbulent WSL. Firstly, the westward shear induced by the zonal velocity perturbations associated with TIWs and other equatorial waves, rather than the meridional velocity shear, plays a crucial role in enhancing the total shear squared (hereafter SS), which is essential in leading to Kelvin-Helmholtz shear instability and hence turbulent mixing (Liu et al., 2019b). This is because the westward shear can nonlinearly magnify the westward shear induced by the mean zonal flow and thus amplify the SS. In contrast, the eastward shear associated with zonal velocity perturbations may suppress and weaken the SS and hence lead to weak mixing. Secondly, the subsurface-intensified tropical instability waves (named as subTIWs; Liu et al., 2019a) or high-order baroclinic waves, which have their zonal velocity core at the subsurface and opposite shear signs above and below the core, can lead to enhanced and weakened mixing on either side, which is essential for the vertically complex pattern of mixing, like the UCL-WSL structure. Additionally, the coupling among multiple equatorial waves with different phases and vertical modes, as well as their interaction with the mean flow, can lead to high-frequency temporal variations (Liu et al., 2020). Particularly, the observed UCL and WSL by the EQUIX experiment are caused by previously identified equatorial mode and subsurface mode tropical instability waves (with central periods of 17 and 20 days, respectively), and subsurface-intensified waves with central periods of 6, 5, and 12 days and velocity maxima at 45-, 87-, and 40-m depth, respectively. In addition, a Kelvin wave with periods of 50–90 days enhances the shear throughout the entire UCL. Liu et al. (2020) again demonstrated that in both the WSL and UCL, most of the largest contributions (either positive or negative) are from the interactions between the slowly varying background zonal flow $\tilde{U}$ (defined as the 45-day low-pass filtered velocity) and zonal oscillating velocities associated with the individual waves.

Liu et al. (2020) found that complex shear and mixing structures similar to the UCL-WSL pattern might frequently occur in the thermocline of Eq140°W due to the saturation of equatorially trapped planetary waves with a variety of dynamical types, temporal periods, meridional and baroclinic modes. The authors extended their study from October 1 to December 31, 2008, and detected more

than 11 UCL-WSL structures with durations ranging from several hours to several days.

However, several questions remain unanswered. First, how frequently do these complex patterns occur? Secondly, what are their thicknesses, durations, and other properties? Thirdly, do these patterns occur in other equatorial regions besides Eq140°W? Answers to those questions are crucial for accurately determining the vertical heat transport and the SST variations in the equatorial region. Therefore, in this paper, we extended the analysis time of Liu et al. (2020) to a much longer period (i.e., 2000–2020) and the study site from Eq140°W to 170°W and 165°E at the equator (hereafter Eq170°W and Eq165°E, respectively), where high temporal resolution (1-h) temperature and velocity measurements are available from the Tropical Atmosphere and Ocean (TAO) project.

In Section 2, we describe the data and methods used to identify UCLs and WSLs. In Section 3, we present the occurrence of UCL and WSL during the study period in terms of their seasonal variations, vertical distribution, thickness, and duration. We also report the results obtained for other equatorial regions represented by Eq170°W and Eq165°E. Finally, we provide conclusions and further discussions in Section 4.

2 DATA AND METHOD

2.1 Data

In this study, we utilize hourly ocean temperature and velocity data at Eq140°W collected by the Tropical Atmosphere and Ocean (TAO) mooring array (McPhaden, 1995). The velocity data are the quality-controlled hourly data with a vertical resolution of 5 m, which was freely downloaded from https://www.pmel.noaa.gov/tao/drupal/disdel/. The temperature data were recorded every 10 min and then averaged hourly. The temperature data were measured at non-uniform vertical intervals, with an average interval of ~8 m above 75-m depth, and ~25 m between 75- and 250-m depth. To address the sparse hourly salinity data, we replaced it with the monthly climatology data averaged over 2004–2022 from the gridded Argo data with a vertical resolution of 10 m (https://www.mmnt.net/db/0/0/ftp.ifremer.fr/ifremer/argo), which is acceptable because the contribution of salinity to density is relatively small (Smyth and Moum, 2013; Liu et al., 2016, 2020). The data were then interpolated and/or extrapolated into 1-m grids using the method described in detail by Liu et al. (2016). Subsequently, hourly density profiles are calculated for the period of January 2000–January 2020.

In addition, to illustrate the velocity features induced by equatorial waves, we also adopt the velocity's variance data from the drifter dataset (Laurindo et al., 2017), which is stored in 0.25°× 0.25° global grids, and was downloaded from the Atlantic Oceanographic and Meteorological Laboratory of the National Oceanic and Atmospheric Administration (AOML/NOAA) at http://www.aoml.noaa.gov/phod/dac/index.php.

2.2 Identification of the UCLs and WSLs

2.2.1 Estimation of the critical Richardson number Ri_c in the TAO profile data

Moum et al. (2009) observed a significant UCL-WSL structure during the EQUIX experiment from November 1–6, 2008 (Fig.1a). Subsequently, Liu et al. (2020) calculated the corresponding SS and the reduced shear squared (hereafter, RSS) based on the TAO data. They found that the mixing structure and the RSS pattern were dynamically consistent (Fig.1b). The RSS is defined as $S^2_{red}=S^2-N^2/Ri_c$, where $N^2=-g\rho_z/\rho_0$ is the squared buoyancy frequency and $S^2=(\partial u/\partial z)^2+(\partial v/\partial z)^2$ is the SS. Here, u denotes the total zonal velocity, which consists of a slowly varying background zonal flow $\tilde{U}$ (defined as the 45-day low-pass filtered velocity in this study), and a disturbance flow u'. Ri_c is the local critical Richardson number. A similar treatment was done for the meridional component. The RSS represents the tendency of the currents to induce shear instability (and hence turbulence and mixing) due not only to the associated velocity shear, but also to the associated density stratification. When RSS $S^2_{red}>0$ (<0), the flow tends to mix (stabilize).

It suggests that, the way to link the shear instability with the TAO profile data is to examine the Richardson number, Ri ($Ri=N^2/S^2$). The shear instability (particularly of the Kelvin-Helmholtz type) is dynamically related to Ri_c, which is suggested to be ~0.25 in theory and many studies. $Ri=Ri_c$ is an equilibrium state for turbulence in a stratified shear flow. When $Ri<Ri_c$, turbulence may be initiated or continue to grow due to shear instabilities. When $Ri>Ri_c$, the steady, parallel and inviscid flow is dynamically stable and any turbulence will decay (Miles, 1961; Rohr et al., 1988). When Ri is close to Ri_c, the flow may lie in the regime subject to marginal instability (Thorpe

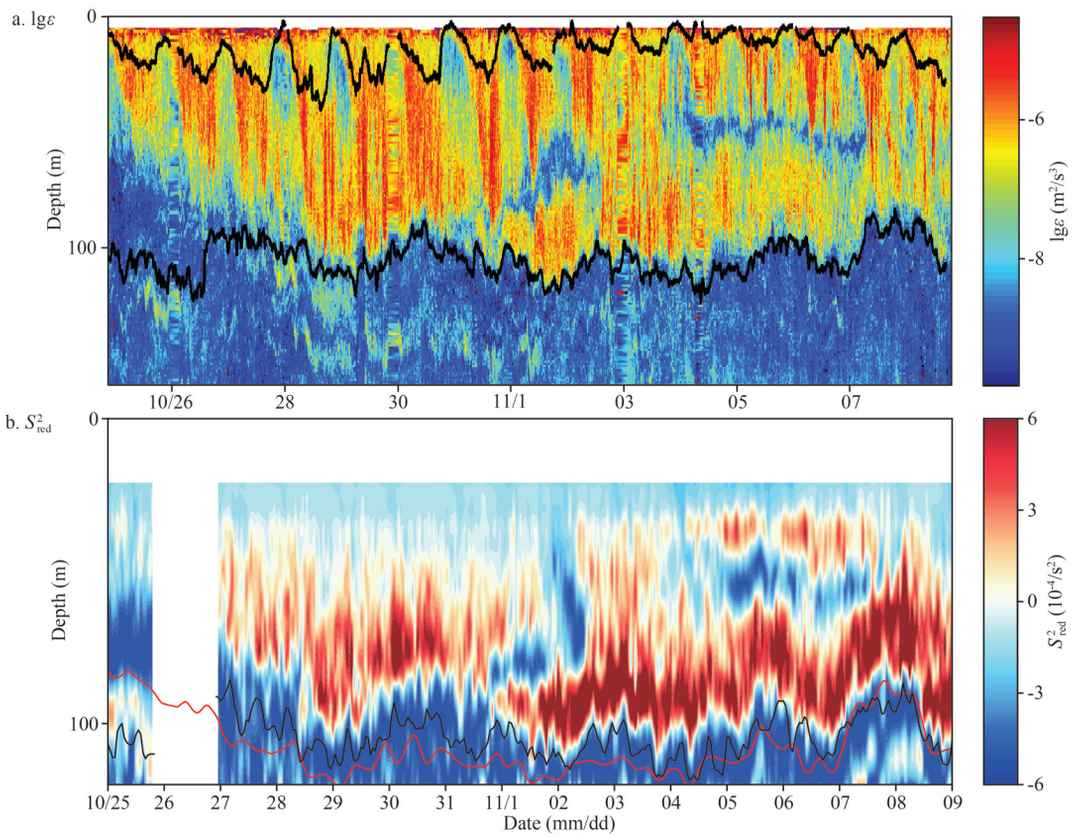

Fig.1 An example of UCL and WSL within the Eq140°W thermocline in 2008

a. depth-time contour plots of dissipation rate of turbulent kinetic energy ε, a copy of Moum et al. (2009)'s Fig.1e. The mixed layer is defined by the upper black line in (a) as the depth at which potential density (ρ) deviates by 0.01 kg/m^3 from its surface value; b. depth-time contour plots of S^2_{red} according to Eq.1. The black and red lines denote the hourly depths of the EUC core (defined as the depth of maximum zonal velocity) and the thermocline center (defined as the depth of 20-°C isotherm), respectively. Reprinted with permission (Moum et al., 2009). Copyright 2009, Springer Nature.

and Liu, 2009). It is found that, when the vertical resolution of data is reduced, this critical number might tend to be larger. For example, turbulence is found at a state of a *Ri* value up to 1/3 in the resolution-reduced (low-resolution) data (Smyth and Moum, 2000); this *Ri* value can be even up to 0.4 at model grids (Cherian et al., 2021). Moreover, Liu et al. (2016) found consistency between occurrence of shear instability and $Ri \leq 0.35$. Therefore, considering the low vertical resolution of the original hourly TAO data (5 m for velocity and >5 m for temperature), Ri_c is chosen to be 1/3 in this study. Finally, the RSS S^2_{red} is formulated as:

$$S^2_{red}=S^2-N^2/Ri_c,\ Ri_c=1/3. \quad (1)$$

Based on the measurement accuracy for velocity and temperature (±5 cm/s and ±0.018 1 °C, respectively, Plimpton et al., 1997; Freitag et al., 2005), the estimated measurement errors of S^2 and N^2 could be small, which hardly affect the calculation of RSS and hence the conclusions of this study. The calculated RSS for the EQUIX period is shown in Fig.1b, which clearly shows the UCL (where $S^2_{red}>0$ in ~60–100 m) and WSL (where $S^2_{red}<0$ in ~40–60 m) during October 24–November 9. The pattern matches well the structure of the UCL and WSL in the observed turbulent kinetic energy dissipate rate (Fig.1a), demonstrating that Eq.1 is an appropriate estimation.

2.2.2 Determination of UCLs (or interior turbulent mixing layers, ITMLs) and WSLs in the TAO profile data

Consequently, we propose a method for defining UCLs and WSLs using TAO profiles. Taking the profiles from October 30, 2008 at 12:00 and November 6, 2008 at 0:00 as examples (Fig.2), we first identify the extreme values of S^2_{red} from the smoothed S^2_{red} profiles. To remove small-scale spikes within the upper thermocline, a 10-m moving smooth is applied. If the maxima (minimal) value of S^2_{red} is positive (negative), the UCL (WSL) will be determined, subject to the following further conditions. If not, no UCL (WSL) exists at that time.

Secondly, further refinements are made to determine the final UCL and WSL. Previous studies have shown that UCL turbulence is commonly present above the EUC core and thermocline center, rather than being directly formed by surface forcing. Therefore, we define the UCL core only when the S^2_{red} maxima is between 20 m and the EUC core. The neighboring depths with positive S^2_{red} are then defined as the UCL (Fig.2a & b). In contrast, the WSL is defined as the layer of negative S^2_{red} that is accompanied by at least one UCL below it. Similarly, its core should locate at the minimal S^2_{red} between 20-m depth and the corresponding UCL core; otherwise, a WSL is not defined. Therefore, a WSL is usually associated with an UCL below it (Fig.2b), but a UCL is not necessarily associated with a WSL (Fig.2a).

It is worth noting that, while the method surely can find those independent UCLs that are above the EUC core and separated from the DCL (Fig.2a), it can also detect turbulent mixing layer that are within the lower part of the DCL (Fig.2b). This indicates that the so-called UCLs detected by the method could be located far above the EUC core. Traditionally, the term "UCL" refers to the layer just above the EUC core; but Liu et al. (2020) have shown that an ITML may not necessarily merge just above the EUC core due to the interaction among complex structured equatorial waves and the mean flows. Therefore, for generality, we refer to the mixing layers detected by our method as interior turbulent mixing layers (ITMLs). It should be noted that some ITMLs, which are located immediately above the EUC core and are separated from the DCL by WSLs, should still be consistent dynamically with the observed UCL in EQUIX.

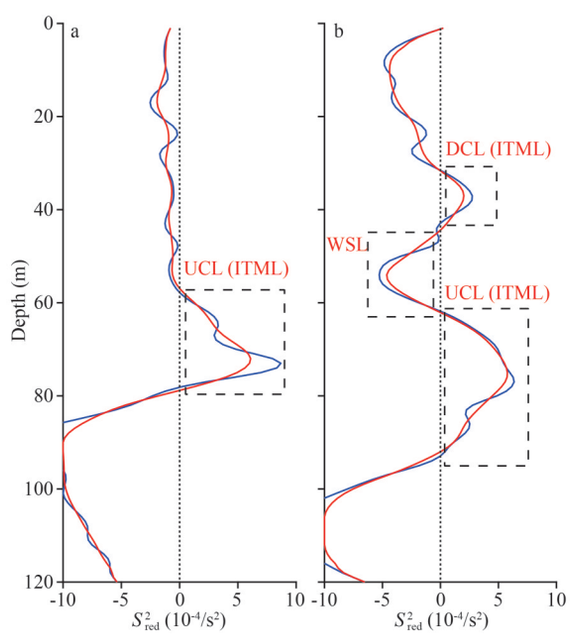

Fig.2 Definitions of UCL (ITML) and WSL based on vertical profiles of RSS on October 30, 2008 at 12:00 (a) and November 6, 2008 at 0:00 (b)

The blue line denotes the original data while the red line denotes the smoothed data. The detected WSL, UCL, and lower DCL are denoted by black dashed boxes. The square box in (a) shows an independent UCL (ITML), while the square boxes in (b) show a UCL (ITML)-WSL structure.

2.3 Occurrence probability and other properties

The occurrence probability of ITML (WSL) is defined as the ratio of the number of profiles of ITMLs (WSLs) to the total number of profiles during the period under study. The climatological seasonal variations of ITML and WSL occurrences are obtained by calculating their occurrence probabilities over each of the 12 months, using the data of January 2000–January 2020. In addition, the vertical distribution of either the ITML or WSL occurrences is obtained by calculating the occurrence probability of their cores at different depths (in 10-m bins) and months. The vertical integration of the occurrence probability of ITML and WSL cores at different depths is approximately equal to their occurrence probability in that month. The occurrence probabilities for thicknesses and durations of the ITMLs and WSLs are calculated in a similar manner.

We note that in order to make the paper easier to read, we summarize the large number of adopted acronyms in Table 1.

3 RESULT

3.1 Occurrence probability and seasonality of the positive RSS S^2_{red} at Eq140°W

Based on the hourly TAO measurements over the years 2000–2020, the occurrence probability of positive S^2_{red} is computed to represent the vertical mixing in the thermocline (Fig.3). The pattern of occurrence probability of positive S^2_{red} (turbulent mixing) is generally consistent with that of the low Richardson number as shown in Fig.6 of Liu et al. (2016). Based on hourly TAO measurements over the years 2000–2010, Liu et al. (2016) calculated the occurrence frequency of low Richardson number (Ri<0.35) to represent the possibility of instabilities, and demonstrated that the annual cycle of the occurrence frequency of low Ri results from the

Table 1 Summary of acronyms

Complete name	Acronym	Complete name	Acronym
Deep-cycle layer	DCL	The changes of reduced shear squared	RSSC
El Niño and Southern Oscillation	ENSO	Shear squared	SS
Equatorial Internal Wave Experiment	EQUIX	Sea surface temperature	SST
0°, 140°W (0°, 170°W; 0°, 165°E)	Eq140°W (Eq170°W; Eq165°E)	Subsurface-intensified tropical instability wave	subTIW
Equatorial mode tropical instability wave	eTIW	Tropic Heat 1	TH1
Equatorial undercurrent	EUC	Tropic Heat 2	TH2
Interior turbulent mixing layer	ITML	Tropical instability wave	TIW
Mixed layer	ML	Tropical Instability Wave Experiment	TIWE
Power spectral density	PSD	Upper core layer	UCL
Reduced shear squared	RSS	Weakly sheared layer	WSL

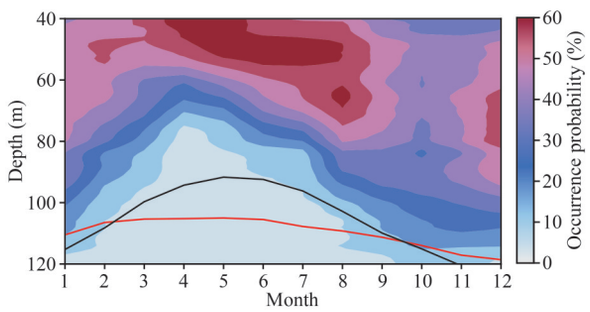

Fig.3 Monthly occurrence probability of positive RSS, S^2_{red} at Eq140°W

The occurrence probability is calculated as the ratio of numbers of positive S over numbers of all non-zero S^2_{red} at each depth-month grid. The black curve denotes the average depth of EUC core and the red curve denotes the average depth of the thermocline center.

shear of EUC and the TIWs (represented by velocity fluctuation with period of 12–40 days).

Similarly, the occurrence of positive S^2_{red} (turbulent mixing) exhibits a significant seasonal variation. The pattern of higher occurrence probability shows a deep extension to ~100 m from late summer to winter, and a subsurface center (at 40 m) from February to August, where the occurrence probability is larger than 30%, and even above 50% in some months. Turbulent mixing occurs at shallower depths in spring and early summer (March–July), when the depth of the EUC core is also at its shallowest stage. The lower vertical bound of the high occurrence probability is generally confined to the centers of the thermocline and the EUC. The seasonal variation of turbulent mixing is influenced not only by the shear of the EUC and equatorial waves, but also by the thermal structure of the upper ocean.

3.2 Occurrence probability and seasonality of the ITMLs and WSLs at Eq140°W

In this subsection, we first show the RSS S^2_{red} during the EQUIX period along with the $\bar{S}^2_{red}$ induced by the slowly varying background zonal flow, as well as the changes of reduced shear squared (hereafter referred to as RSSC) ΔS^2_{red} (Fig.4). In the layer above ~100-m depth, $\bar{S}^2_{red}$ is around 0 (Fig.4b), confirming that this layer is marginally stable (Smyth and Moum, 2013). As a result, the occurrence of turbulent mixing depends primarily on ΔS^2_{red} (Fig.4c). For example, in the UCL during November 1–6, the formation of this turbulent mixed layer mainly depends on the positive RSSC ΔS^2_{red} (Fig.4c). This shows that shear instability is well related to turbulent mixing therein. The occurrence probability of ITML (not the previously defined UCL) during the EQUIX period, calculated as the ratio of the number of profiles containing ITMLs to the total number of profiles, is 78.2%; and that of the WSLs is 43.6% (Figs.1 & 5). This result seems higher than visual estimations because the ITML in the present study includes not only turbulent mixing of the UCL layer, but also some mixing of the lower part of the DCL or the DCL mixing fused with independent UCLs.

We then extend the analysis period to January 1, 2000–January 1, 2020, and recalculate the occurrence probability of both ITML and WSL at each depth (Fig.5). The results show that the occurrence probability of ITML is 67.8%, indicating that ITML is present throughout the thermocline at Eq140° W. In contrast, the occurrence probability of WSL is 26.6%, which is about 2 times less than that of the ITML. This is because a WSL can only be identified when it is accompanied by an ITML-WSL structure, while the ITML can exist independently. The results demonstrate the persistence of ITML and WSL at Eq140°W.

A prominent feature is the biannual seasonal variation of the occurrence probability of the ITMLs

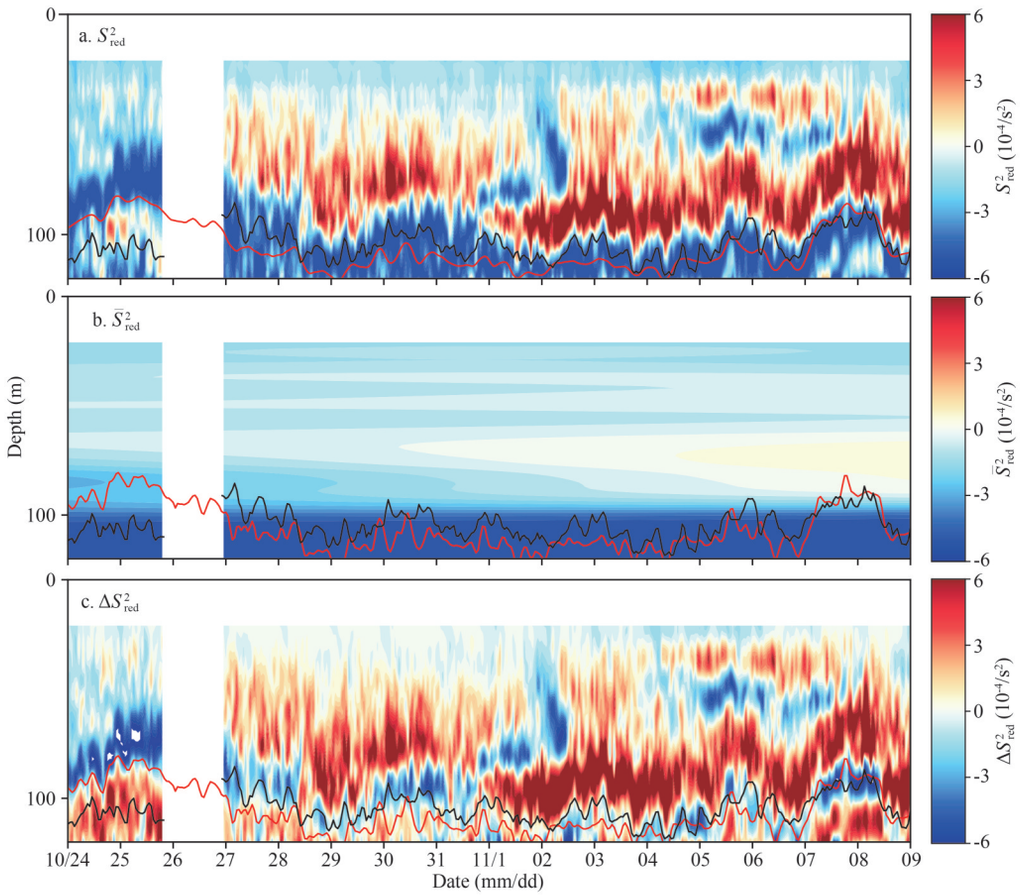

Fig.4 RSS and its contributions at Eq140°W in 2008

a. RSS from the SS and buoyancy frequency squared, calculated with Eq.1; b. RSS from the slowly varying background shear squared and buoyancy frequency squared, calculated as $\bar{S}^2_{red}=\bar{S}^2-\bar{N}^2/Ri_c$; c. RSSC from both the shear squared changes and buoyancy frequency squared changes, calculated as $\Delta S^2_{red}=S^2_{red}-\bar{S}^2_{red}$. a=b+c. The black and red lines denote the hourly depths of the EUC core and the thermocline center, respectively. Shown are for the EQUIX period at Eq140°W.

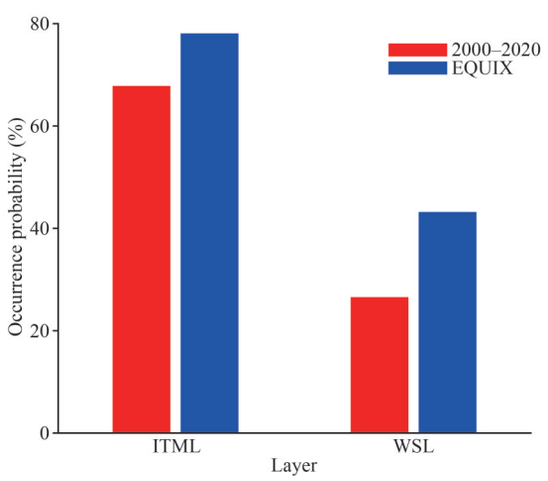

Fig.5 Total occurrence probability of ITML and WSL at Eq140°W

The occurrence probability is calculated during the EQUIX (blue) period and over the years 2000–2020 (red).

(Fig.6a). Within the thermocline, more ITMLs are found in boreal late summer to winter, while relatively fewer ITMLs are found in boreal spring. There are also fewer ITMLs occurring in October. The occurrence probability of ITML peaks in June and December respectively, with a value of about 75% in both months; it also shows two minimum peaks, one in April with a value of about 55%, and the second in October with a value of ~62%.

Figure 6b further shows the distribution of the ITML core across different depths and months. The depths with a high occurrence probability of ITML are located ~30–70 m above the seasonally varying EUC core. Wherein, the high-frequency of ITML is located at the shallowest depths (in the range of 40–80 m, but mostly in 40–60-m depth) in spring and early summer (March–June), corresponding to the months of shallowest EUC core. In the concentrated depths (40–60 m), the ITMLs account for up to 20% or more during these months, while in late summer to winter (July–February), the high-frequency distribution of ITML becomes deeper, ranging 40–

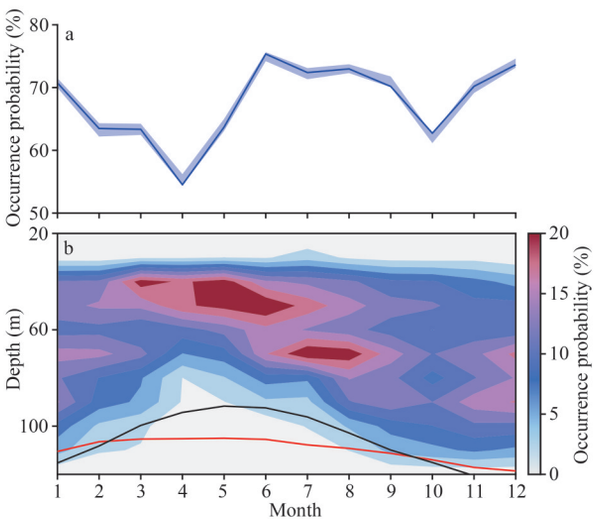

Fig.6 Monthly occurrence probability of ITML (a) and depth-month plots of occurrence probability of ITML cores at Eq140°W (b)

Shown are counts in 10-m bins. In (a), shading denotes 95% bootstrap confidence levels; in (b), the black and red lines denote the monthly climatological depths of the EUC core and the thermocline center, respectively.

120-m depth, but is concentrated in 60–100-m depth. Within these depths, the ITML cores can also account for up to 20% of all the ITMLs in these months. This shows that ITML also has obvious seasonal variations in its vertical distribution. This seasonal variation arises for the same reasons as the seasonal variation of low Richardson numbers or positive RSSs, as mentioned in Section 3.1.

This vertical and seasonal picture (Fig.6b) also reflects some features of the EQUIX observations (Fig.1). For example, most of the larger turbulent mixing, formed as a combination of the UCL mixing and the upper DCL mixing, observed on October 27–November 1, 2008, occurred in 60–80 m. In addition, the locations of the strongest turbulent mixing in the UCL, which were separated from the upper DCL by the WSL on November 1–9, 2008, were mostly located in a deeper layer, i.e., 80–100 m. All of those locations are consistent with the peaks shown in Fig.6b. Figure 6b further suggests that ITMLs should occur frequently between 60- and 100-m depth from November to the February of the following year. ITMLs should also occur frequently between 60- and 80-m depth in March and June–August. On average, there are relatively fewer ITMLs in October.

Figure 6b also shows that since most ITML cores occur at shallower depths (40–60 m) during boreal spring, they might merge with the DCLs and form a joint turbulent mixing structure, similar to what happened during October 28–30, 2008 (Fig.1a).

The seasonal variation of the overall occurrence of WSL within the thermocline is similar to the ITML, although it shows more of an annual cycle (the secondary minimum in October is not significant): more WSLs are found in boreal late summer to winter, while relatively few WSLs are found in boreal spring to early summer (Fig.7a). The occurrence probability peaks in September and January, reaching a value of about 36%, and shows lowest values in April to June, which is only about 15%. The maximum values in September and January are more than twice as high as the minimum value in May. Additionally, the occurrence probability of WSL also has significant seasonal variations in its vertical distribution (Fig.7b). Firstly, over all months, there seem to be two concentration layers of the relatively high occurrence of WSLs, with the first being at 20–35-m depth and the other at 50–85-m depth. The occurrence probability of WSL cores at the shallower layer is higher in August, September, and January, but is lowest in spring and early summer (April–June); however, this concentration layer accounts for only less than 5% of the total WSLs. Most WSLs occur in the deeper concentration layer (50–85 m). The occurrence probability of this layer is higher in late summer to winter (July–February), with a value of

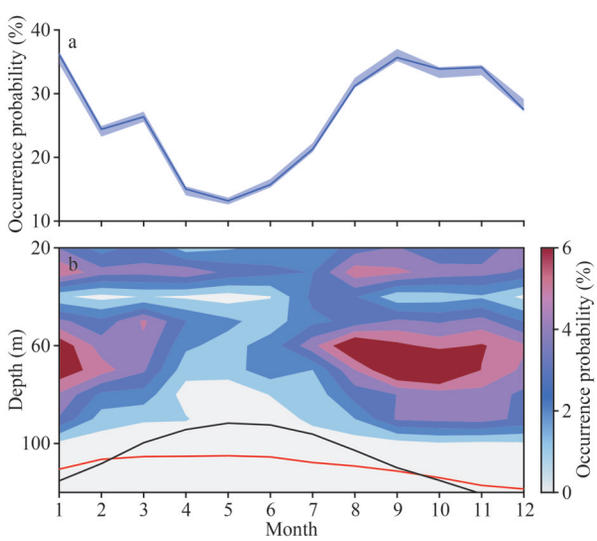

Fig.7 Monthly occurrence probability of WSL (a) and the depth-month plots of occurrence probability of WSL core at Eq140°W (b)

Shading denotes 95% bootstrap confidence levels. The black and red lines denote the hourly depths of the EUC core and the thermocline center, respectively.

larger than 6% per 10-m thick layer. Whereas, a prominent feature is that higher occurrence only happens from later summer to winter during this layer (August–February), but almost no WSLs are found in this layer during spring. This seasonal variation of the vertical distribution of WSLs is consistent with the ITMLs, both of which form important complex mixing structures. This spatial pattern is also confirmed by the EQUIX observations, where the core of WSL structure was around 80-m depth on November 1–2, 2008 and at 55-m depth during November 4–7, 2008, respectively.

The above results demonstrate the persistence of ITMLs and WSLs at this site. As argued by Liu et al. (2020), their occurrence probability is due to the coupling among multiple temporal and spatial scale equatorial waves in different phases, particularly high-order baroclinic waves, and mean equatorial currents. Liu et al. (2020) found that multiple-temporal-scale (from 3 to 25 days) equatorial waves were manifested primarily as zonal velocity oscillations with maximum amplitudes (from 10 to 30 cm/s) occurring at different subsurface layer depths (from the surface to 85-m depth) above the seasonal thermocline. These waves are most significant during the TIW seasons, i.e., from boreal summer to winter. Particularly, the monthly occurrence probability of ITMLs is well correlated with the multi-year monthly average TIW kinetic energy (KE) at Eq140°W, which shows that the TIW KE is large in late summer to winter, small in spring and has a minimum peak in October (Liu et al., 2016). The consistency between them suggests that the occurrence of ITMLs should be greatly contributed by equatorial waves.

3.3 Variation in the thickness and duration of the ITMLs and WSLs at Eq140°W

The ITML-WSL structure, or either of them, can emerge due to the couplings of equatorial waves, and the duration of the ITML-WSL structure depends on how long the interacting equatorial waves persist in their favorable phases simultaneously. To further investigate the strength of ITMLs and WSLs, we analyzed the temporal variation and spatial distribution of the ITMLs' and WSLs' thicknesses and durations. Figure 8a–b shows that the thickness of ITML range 5–85 m, but concentrated in 15–55 m (accounting for more than 80%). The proportion of thicker ITMLs (>35 m) is large, accounting for about 60%. For reference, the thickness of the observed strongly turbulent UCL by the EQUIX experiment during November 1–4, 2008 was about 50 m thick. The present results indicate that the vertical extension of mixing in the ITML is generally large within the Eq140°W thermocline. However, the thickness of the WSL structure is much less than that of the ITML. Figure 8c–d shows that the thickness of each WSL structure is concentrated in 5–35 m, accounting for about 76%. During the EQUIX period, the average thicknesses of the WSLs during November 1–2, and during November 4–7, were about 25 m, being consistent with the present results. As defined in the Method section, the existence of any WSL is accompanied by an ITML below. Therefore, in any of the joint ITML-WSL structures, even if the ITML mixing is strong, the presence of the WSL makes it difficult for the UCL in the ITML to merge with the surface forcing-driven upper layer mixing, indicating again that they are generated by interaction among equatorial waves and the mean flows.

We further investigate how the density distribution of ITML and WSL thicknesses varies with months. Obvious seasonal variations are found (Fig.8b & d). As can be seen from Fig.8b, thinner ITMLs (with thickness between 20 and 40 m) prevail in spring to early summer, while a wide thickness range (15–80 m) of ITMLs occur more evenly in late summer to winter. However, the prevailing thickness seems larger in spring (15–30 m), accounting for up to 25% or more, while the prevailing thickness seems smallest during July, August, December, and January (10–25 m). In contrast, the seasonal variation of WSL thickness is different (Fig.8d). The highest prevailing thickness of WSLs (20–30 m) occurs in spring and early summer, which accounts for 35% or more, followed by the thickness range of 10–25 m in autumn, and the thinnest thickness range of 10–20 m in winter.

The duration of each ITML (Fig.9a–b) is mainly concentrated within 3 days. Such ITMLs account for more than 70% of all ITMLs. However, about 15% of the detected ITML structures lasted for a period of longer than seven days. As argued by Liu et al. (2020), the periods of the equatorial waves vary from days to more than a month, usually making the duration of any WSL or ITML, which is coincidentally generated by equatorial waves' interactions, very short. If the period of one or several equatorial waves involved in the interaction is long, the duration of WSL or ITML may be long; and conversely, if the period of the equatorial waves is short, the duration of WSL or ITML will be short.

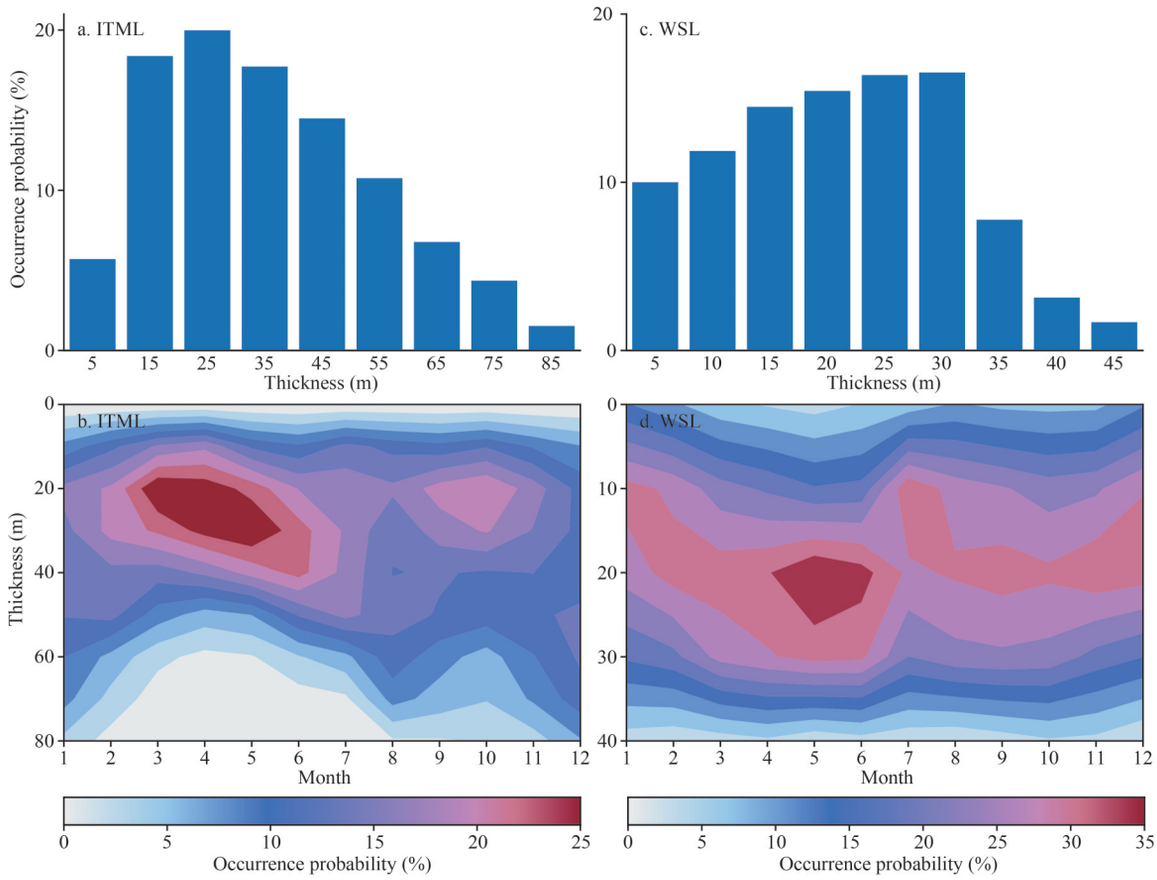

Fig.8 Variations in the thickness of the ITMLs and WSLs at Eq140°W

Histogram of the occurrence probability of the thickness of the ITML (a) and WSL (c) structures. Monthly occurrence probability of different thicknesses of the ITML (b) and WSL (d) structures. The occurrence probability of the ITML thickness is calculated every 10 m, while the WSL thickness for every 5 m, and each tick is obtained as the middle value.

Therefore, these long-duration ITML structures should be maintained by stable joint structure of equatorial waves, particularly by the long-period Rossby, Rossby-gravity and Kelvin waves. Usually, the duration of the WSL is shorter than that of ITML. Most WSL structures (80%) have a duration of less than two days (Fig.9c). Similarly, the short duration of the ITML-WSL structure is likely due to the fact that they are formed by the joint action of equatorial waves with multiple time scales; on the other hand, since WSLs locate on the upper layers, they could be occasionally split into short segments by the diurnal cycle DCL turbulent mixing, and hence show short time scales. In contrast to the thickness or occurrence probability, the duration of the ITML and WSL structures seem not to be significantly modulated by different seasons (Fig.9b & d).

3.4 Occurrence probability and seasonality of ITMLs and WSLs in other equatorial sites

In the above subsection, we have demonstrated that ITML and WSL persist at Eq140°W due to interactions among equatorial waves and the background shear flow. However, it is not yet known whether ITML and WSL structures are also present in other regions of the equator, or how frequent if they occur, due primarily to a lack of direct turbulence observations. The variance of the surface zonal velocities (Laurindo et al., 2017) over the Pacific Ocean is shown in Fig.10. It demonstrates that the equatorial wave-induced velocity fluctuation is large throughout the Pacific basin. Therefore, we hypothesize that turbulent mixing should also be frequent at other equatorial sites. In this subsection, we extend our study to the TAO observation sites at Eq170°W and Eq165°E.

To begin with, like Eq140°W, we select two time periods, September 15–January 15, 2016, for Eq170°W and September 15–January 15, 2018, for Eq165°E, to investigate the occurrence of positive S^2_{red} (Fig.11). The results show that positive RSSs are also prevalent in the thermocline at these two sites.

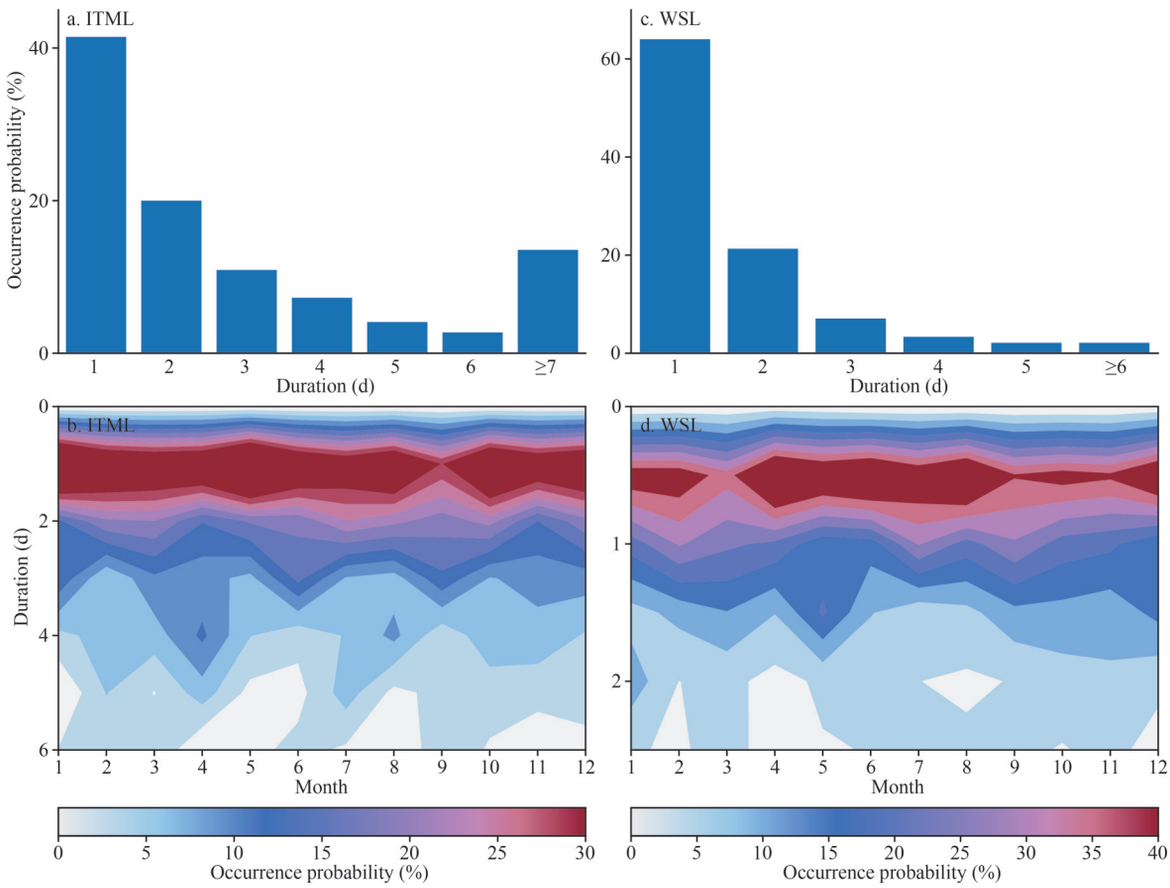

Fig.9 Variations in the duration of the ITMLs and WSLs at Eq140°W

Histogram of the occurrence probability of the duration of the ITML (a) and WSL (c) structures. Monthly occurrence probability of different duration of the (b) ITML and (d) WSL structures.

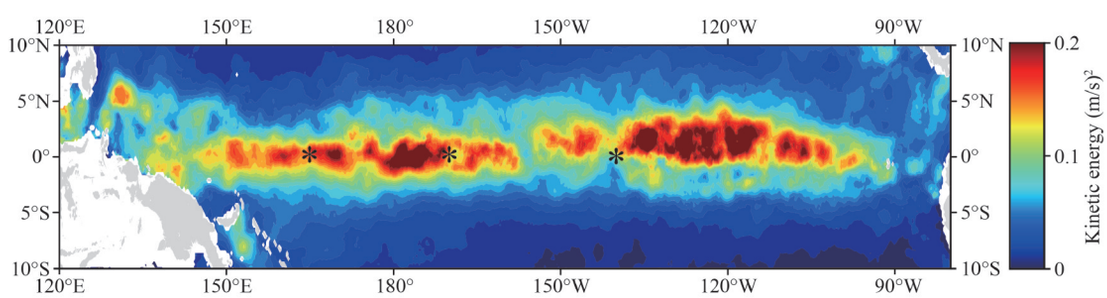

Fig.10 Current variance (eddy kinetic energy) of surface zonal velocities in the Pacific Ocean from Laurindo et al. (2017)'s drifter data

* indicates the TAO observational sites that are analyzed in this study.

In addition, in the layer above ~100-m depth, the $\bar{S}^2_{red}$ is also around 0 (Fig.12), demonstrating that this layer is also marginally stable, and the positive RSSs, and hence the ITMLs, are also occasionally generated by equatorial waves.

We also calculated the occurrence probability of the ITML and WSL structures at Eq170°W from January 1, 2001 to January 1, 2020, and at Eq165°E from January 1, 2000 to January 1, 2019 (Fig.13). The occurrence probabilities of ITML at Eq170°W and Eq165°E are about 53% and 48%, respectively, which are ~15% and ~20% less than that at Eq140°W (which is 68%). The occurrence probability of WSL structures also varies significantly across regions. It is significantly higher at Eq165°E (28%) and Eq140°W (27%) than at Eq170°W (15%), indicating that there are many obvious joint ITML-WSL structures at Eq165°E. In

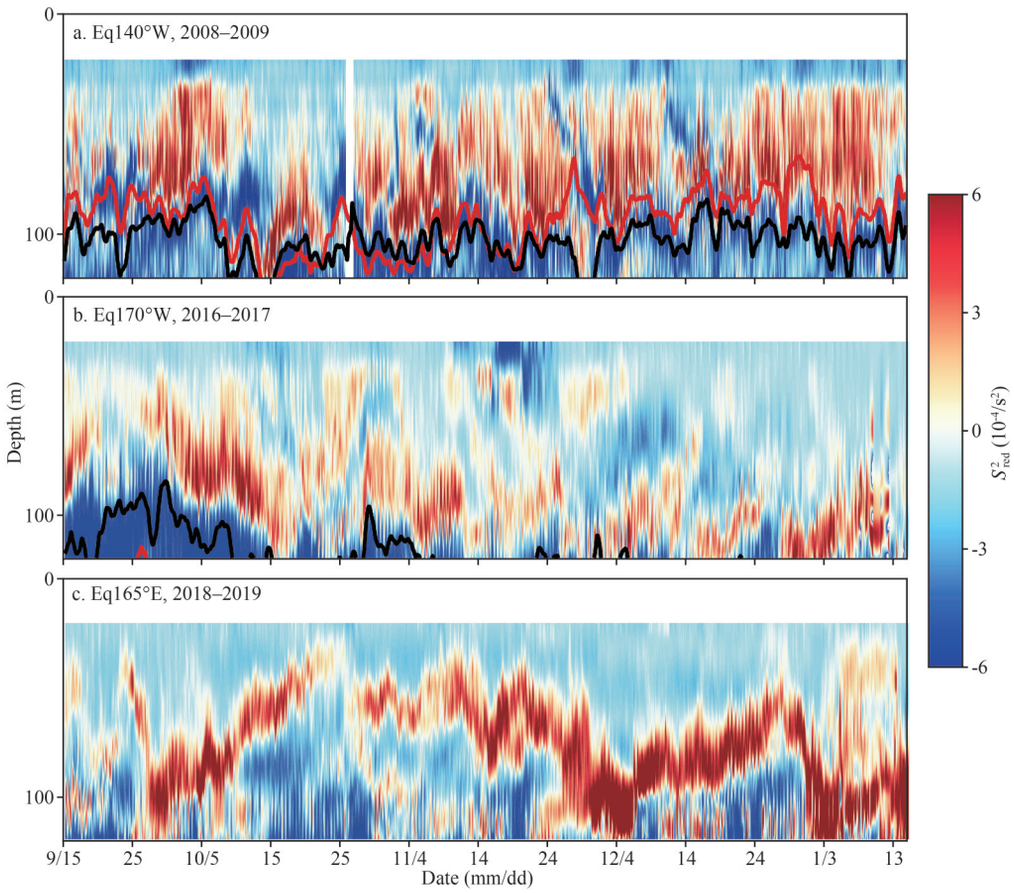

Fig.11 RSS induced by the total shear squared and the total buoyancy frequency squared at three equatorial sites

a. at Eq140°W; b. Eq170°W; c. Eq165°E, calculated for a 4-month period. The black and red lines denote the mean depths of the EUC core and the thermocline center, respectively (those for the Eq170°W and Eq165°E are beyond the figure scope).

general, the persistence of ITML and WSL structures is not only present at Eq140°W but also at Eq170°W and Eq165°E.

The occurrence probability of ITML at Eq170°W also exhibits a significant biannual seasonal variation (Fig.14a). The results show that it is also more likely to occur in late summer to winter, when the occurrence probability can be close to 60% near the two peak months (February and August); it occurs relatively less frequently in late spring to early summer (April and July, with a minimum in June), but still shows a high occurrence probability (>40%). This biannual seasonal variation generally resembles that of Eq140°W. Similarly, due to its high occurrence of ITML, Eq170°W is also likely a significant hotspot of thermocline mixing, which is worth intensive measurements.

The overall seasonal variation (annual cycle) of WSL occurrence at Eq170°W is similar to that of ITML. The results reveal that the occurrence probability of WSL reaches more than 20% in late autumn to winter. It also shows that the months of the lowest occurrence of ITML and WSL (both in June) seem to be one- or two-month later than that of Eq140°W.

However, unlike these two regions, the occurrence probabilities of ITMLs and WSLs at Eq165°E are much lower in the second half of the year (June–December) than in the first half (January–May). On average, the occurrence probability in the first half-year is nearly 20% higher than that in the second half-year. The reasons for this feature require further studies.

At Eq170°W and Eq165°E, the vertical distribution of the cores of ITML and WSL moves downward along with the deepening of the EUC core (Fig.14b, d, f, & h). At Eq170°W, the ITML and WSL cores are located about 30–100 m and 50–90 m above the seasonally varying EUC core, respectively. Both the vertical direction of ITML and WSL structures have significantly similar seasonal variations to Eq140°W, with deeper

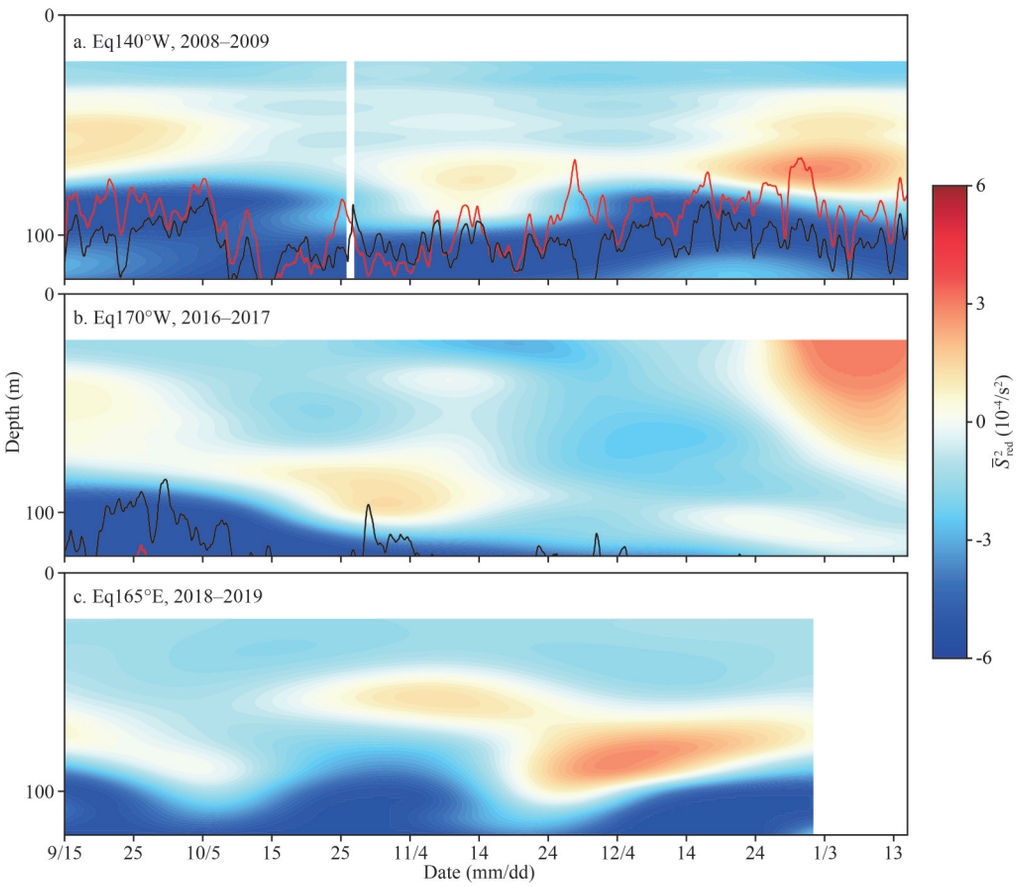

Fig.12 RSS from the background shear squared and background buoyancy frequency squared at three equatorial sites

a. Eq140°W; b. Eq170°W; c. Eq165°E; calculated for a 4-month period. The black (in a and b) and red (in a) lines denote the hourly depths of the EUC core and the thermocline center, respectively.

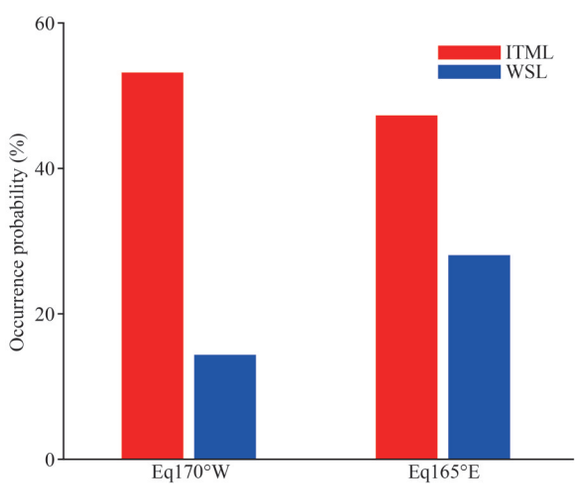

Fig.13 Total occurrence probability of ITML (red) and WSL (blue) at Eq170°W and Eq165°E

The occurrence probability at Eq170°W and Eq165°E are calculated for the years 2001–2020 and 2000–2019, respectively.

distributions in late summer to winter, concentrated between 100–140 m and 90–120 m, respectively. They also show shallower distributions in spring and summer, concentrated between 55–90 m and 60–80 m, respectively. In contrast, the ITML and WSL cores at Eq165°E are located about 50–150 m and 60–120 m above the seasonally varying EUC core, respectively. Compared to the Eq140°W and Eq170°W, the seasonal variation of ITML and WSL at Eq165°E is not concentrated in the vertical direction; instead, the vertical extension of both the ITMLs and WSLs is much wider, and does not show obvious seasonal variations.

Figure 15 shows the probability density and seasonal variation of the thickness of ITML and WSL structures at Eq170°W and Eq165°E. At Eq170°W, the thickness of the ITML is similar to the overall distribution at Eq140°W, concentrated between 15–55 m and accounting for more than 85%. Slightly different from Eq140°W, the WSL structure is thicker, concentrated in 15–45 m, with a ratio of nearly 70%. Meanwhile, the thickness of the ITML at Eq165°E is a little thinner than in the other two regions, with a concentration in 5–25 m and accounting for more than 85%. This suggests a

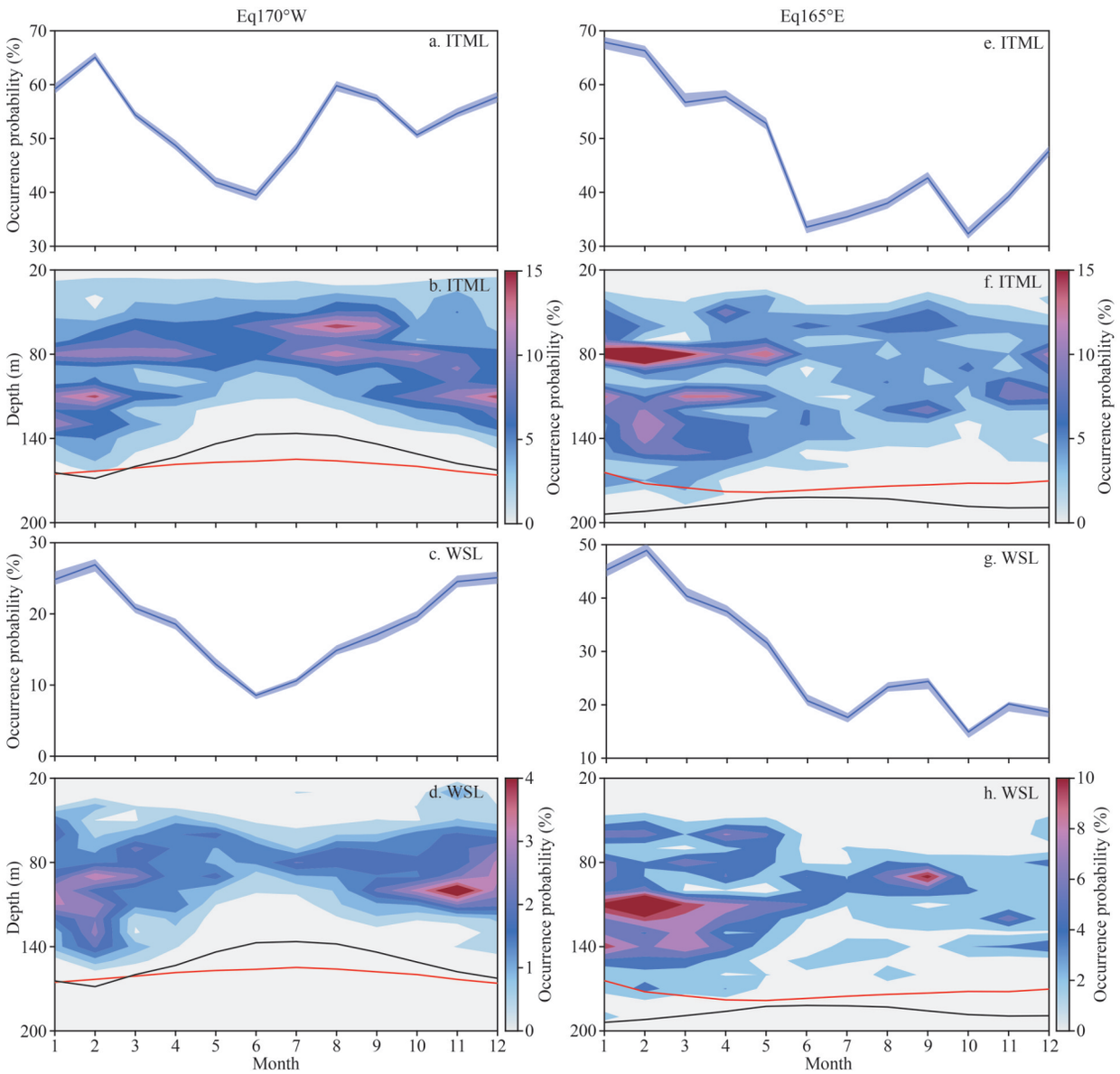

Fig.14 Monthly and vertical variation of occurrence probability of ITML and WSL

(a–d) as in Fig.6 and Fig.7, but at Eq170°W (left panel), monthly occurrence probability of ITML (a) and WSL (c). Depth-month contour plots of occurrence probability of ITML (b) and WSL (d) core depth, the black and red lines denote the hourly depths of the EUC core and the thermocline center, respectively (see caption of Fig.4); (e–h) as on the left panel, but at Eq165°E (right panel). In (a, c, e, and g), shading denotes 95% bootstrap confidence levels.

smaller vertical extension of mixing in that area. On the contrary, the thickness of the WSL at Eq165°E is a little thicker than in the other two regions, concentrated in 15–55 m and accounting for more than 80%. There is weak seasonal variation in the thickness of the ITML at Eq170°W, where 20%–25% and more of the ITML is concentrated in 15–40 m in summer and early autumn, and 15–30 m in other seasons. Besides, the thickness of the WSL in Eq165°E also has a few special seasonal variations. In late autumn and early winter, the prevailing thickness of WSL is thinnest, concentrated in 5–15 m (20%–25% and above) and 25–40 m (17%–25%), while in spring, there is also a portion of WSL structures concentrated in 5–15 m, with a rate of about 20%. In September, the thickness of WSL is thickest, with about 20% concentrated in 45–60 m. In other months, the thickness of WSL is concentrated in 30–50 m (20%–25% and above). This seasonal variation in thickness is very different from that at Eq140°W, because the intensity of the ITML produced by the interaction between different

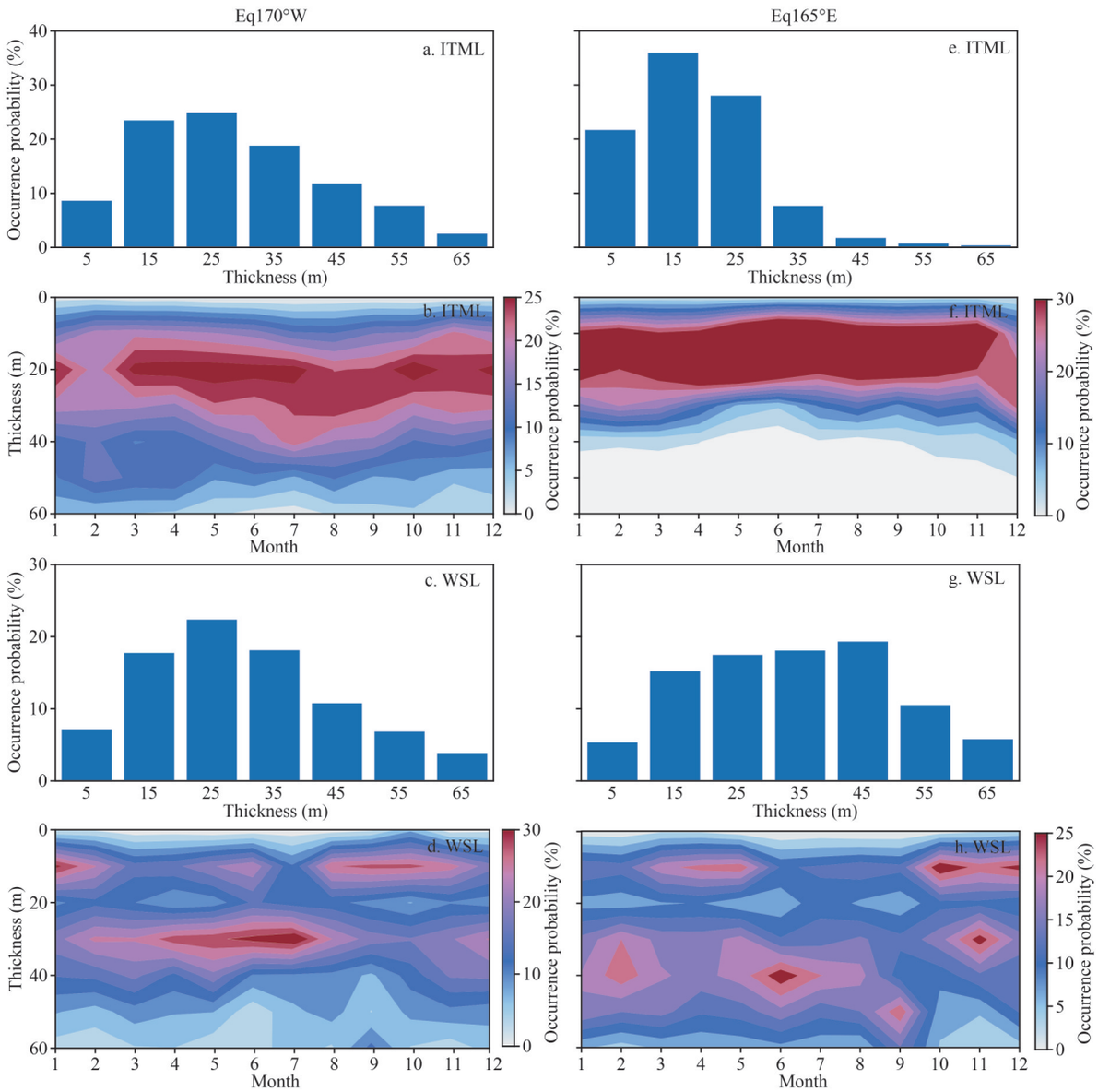

Fig.15 Histogram of the occurrence probability and monthly occurrence probability of the thickness of ITML and WSL

Histogram of the occurrence probability of the thickness of the ITML (a) and WSL (c) structures. Monthly occurrence probability of different thicknesses of ITML (b) and WSL (d) at Eq170°W (left panel). (e)–(h) as on the left, but at Eq165°E (right panel). The occurrence probability of the ITML and WSL thickness are calculated every 10 m.

equatorial waves and the mean flow varies in different regions. In contrast, there is no significant seasonal variation in the thickness of the WSL at Eq170°W, and both the ITML and WSL at Eq165°E. At Eq170°W, the prevailing thickness of WSL is concentrated around 15 m (with 25%) and between 25–35 m (with 25%–30% and more) in different seasons.

We also analyze the probability density of the distribution of the two structures' duration and their seasonal variations in these two regions (Fig.16). The distribution of the duration of ITML and WSL is not significantly different from that of Eq140°W in either Eq170°W or Eq165°E. In these two regions, most ITMLs (80% and 79% at Eq170°W and Eq165°E, respectively) last for 3 days, and about 7% of ITMLs are longer than 7 days. Meanwhile, most WSLs (90% and 78% at Eq170°W and Eq165°E, respectively) last for no more than 2 days. As argued earlier, the reason for the short duration of ITMLs and WSLs is due to the shorter periods of one or more equatorial waves that generate them. Only in Eq165°E, the duration of WSL is slightly longer overall than the other two

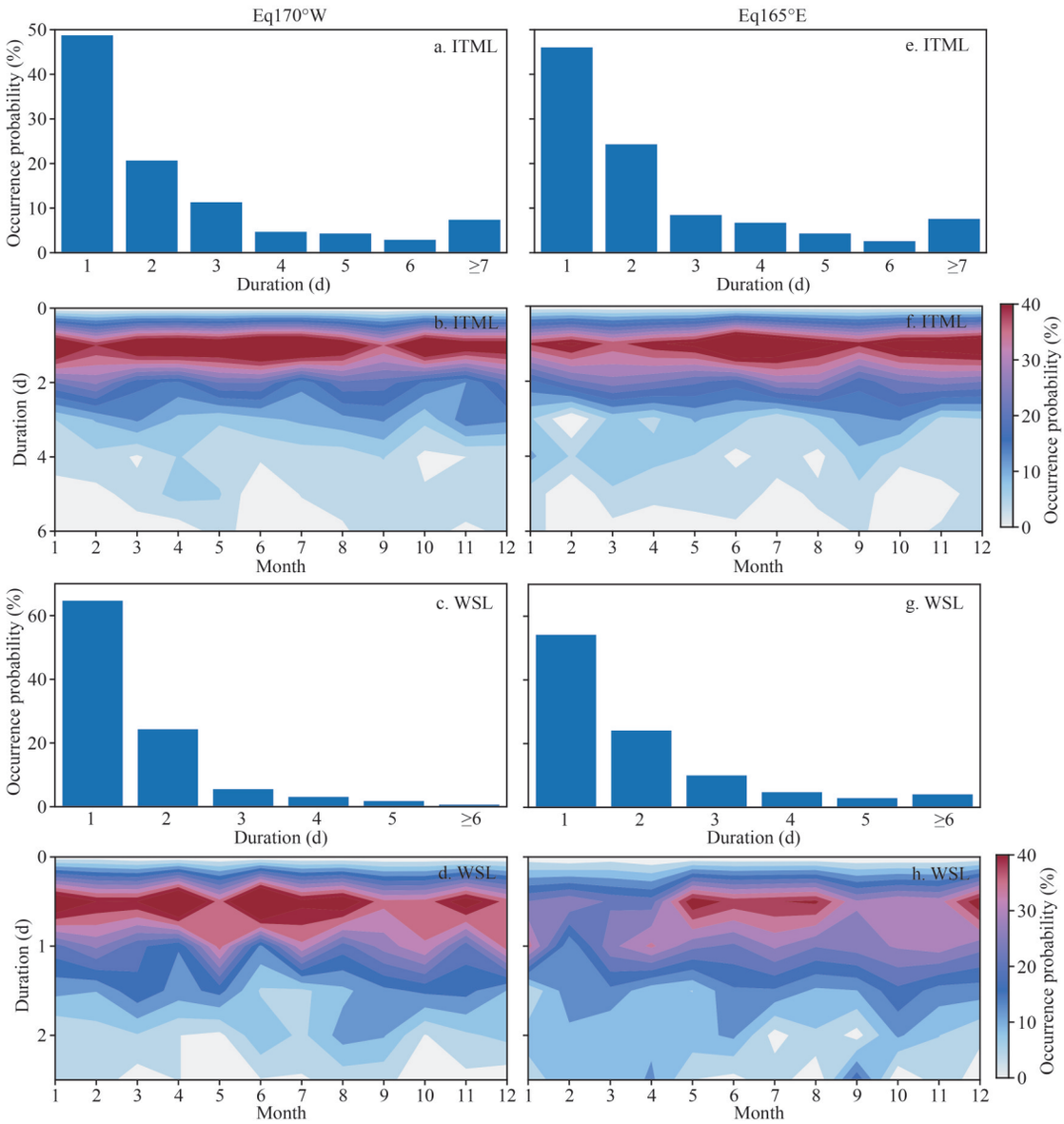

Fig.16 Histogram of the occurrence probability and monthly occurrence probability of the duration of ITML and WSL

Histogram of the occurrence probability of the duration of the ITML (a) and WSL (c) structures. Monthly occurrence probability of different duration of ITML (b) and WSL (d) at Eq170°W (left panel). (e)–(h) as on the left, but at Eq165°E (right panel). The spacing is selected as in Fig.9.

regions. Here the joint ITML-WSL structure is supposed to be influenced by the more stable joint action of equatorial waves. Moreover, the duration of ITML and WSL is also unaffected by seasonal variations at Eq170°W and Eq165°E.

4 SUMMARY AND DISCUSSION

This study, based on the framework proposed by Liu et al. (2020), demonstrated that the joint UCL (ITML) -WSL structures, or either the UCL or the WSL, are formed by coupling among multiple-temporal-scale equatorial waves and the mean equatorial flow, we further investigate the occurrence properties of these complicated shear and mixing structures in the Eq140°W thermocline, as well as that at Eq170°W and Eq165°E. We pay special attention to the mixing structures' temporal and vertical variations. Following this, in order to understand the intensity of mixing and the intensity influenced by the combined effect of equatorial waves, we also discuss the thickness and duration of the ITML and WSL structures.

The occurrence probability of ITML at Eq140°W over 2000–2020 is 67.8% and that of WSL is 26.6%, which clearly demonstrates that there is indeed a

large amount of shear and turbulent mixing structure at the thermocline of Eq140°W. In addition, the occurrence probability of ITML and WSL has obvious biannual seasonal variations, which is high in boreal late summer to winter, and low in spring.

In the thermocline, the ITML and WSL cores are centered ~30–70 m and ~40–80 m above the seasonally varying EUC core, respectively. The ITML and WSL also exhibit obvious seasonal variations in the vertical direction. The high frequency of ITML and WSL cores is distributed more shallowly in spring and early summer (March–June), ranging from about 40–60 m and 20–35 m, respectively, while in late summer to winter (July–February), the high-frequency distribution of ITML and WSL becomes deeper, concentrated between 60–100 m and 50–85 m, respectively.

Furthermore, at Eq140°W, over 80% of the ITMLs have a thickness concentration between 15 and 55 m. In contrast, the thickness of the WSLs is much smaller than that of the ITML structure, with ~76% of WSLs concentrated in 5–35 m. Moreover, the thicknesses of ITML and WSL structures have obvious seasonal variations at Eq140°W. The thickness of ITML is concentrated in 20–40 m from spring to early summer and in 15–80 m from late summer to winter. In contrast, the seasonal variation of WSL thickness is different. The prevailing thickness of WSL is 20–30 m and mainly occurs in spring and early summer, followed by 10–25 m in the autumn and the thinnest (10–20 m) in winter.

Moreover, 70% of ITML structures have a duration mainly concentrated within 3 days, while 80% of WSL structures last less than two days. However, approximately 15% of ITML structures last longer than seven days. There are no significant seasonal variations in the duration of ITML and WSL.

In a conclusion, the high occurrence probability of ITML demonstrates that ITMLs, hence interior turbulent mixing in the thermocline, are persistent at Eq140°W in the equatorial eastern Pacific. This conclusion is supported by the short durations and variable thicknesses of the ITML and WSLs. Because the period of equatorial waves varies from a few days to a month and the core depths of the waves vary from the surface to just above the EUC core, the joint effect of all the favorable waves and the mean flow could only maintain a short time and a certain depth range to be favorable for shear instability and mixing. However, these conditions can be frequently and occasionally satisfied, which leads to the persistence of the ITMLs.

In addition, we find that the occurrence probabilities of ITML and WSL at Eq170°W are 53% and 15%, respectively, corresponding to 48% and 28% at Eq165°E. Given the strong equatorial wave within the equatorial band, it is possible that the entire equatorial thermocline shows the same situation as the three sites analyses here, i.e., the ITML and WSL are prevalent. The biannual seasonal variation in the occurrence probability of ITML and WSL at Eq170°W is generally consistent with that at Eq140°W. However, it differs in Eq165°E. The ITMLs and WSLs show a much lower occurrence probability in the late half-year (June–December) than in the early half-year (January–May). The possible reasons for the different features here from the other two sites may be associated with differences in the equatorial waves, the ENSO-related processes, or the basic temperature and flow states. For example, the TIWs are energetic in the eastern equatorial Pacific but not in the western equatorial Pacific; in addition, Eq165°E is at the eastern edge of the Pacific warm pool, where the mixed layer and EUC are deeper. This issue is worth further study.

Compared to Eq140°W, the ITML and WSL cores have an overall downward shift in their vertical distribution with deepening EUC depth at Eq170°W and Eq165°E. At Eq170°W, the vertical distribution of ITML and WSL shows significant seasonal similarity to Eq140°W, but no obvious seasonal variation is observed at Eq165°E. At Eq170°W, the thicknesses of ITML and WSL structures are concentrated in 15–55 m and 15–45 m, respectively, which are basically the same as those at Eq140°W. However, the thickness of ITML at Eq165°E (concentrated in 5–25 m) is generally thinner than the other two regions, while that of WSL (concentrated in 15–55 m) is thicker. The thickness of ITML at Eq170°W and WSL at Eq165°E both show weak seasonal variation and differs from that of Eq140°W. In contrast, there is no significant seasonal variation in the thickness of WSL at Eq170°W nor in ITML at Eq165°E. The duration properties and seasonality of the two structures at Eq170°W and Eq165°E are not very different from those at Eq140°W. In summary, both the ITMLs and WSLs are also persistent in both regions, and given their short durations and variable thicknesses, they can also be explained by the interaction between the persistent equatorial waves and equatorial currents.

We note that the vertical resolutions of the original velocity and temperature data might affect the determination of the WSL and IMTL, but they do not essentially change the primary features as revealed here. This is because either the vertical extension of most of the mixing events (or WSL and IMTL), or the vertical extension of most of the equatorial waves' characteristic vertical scale, is larger than the vertical resolution of the data.

The persistent mixing bursts represented by the persistent ITMLs could have significant effects, potentially resulting in overall enhanced mixing above the thermocline center and providing an additional mechanism for diapycnal mixing and downward heat transfer in this region. However, the mixing effects need to be quantified and properly represented in numerical models that are unable to resolve the small vertical scale of the equatorial waves. This may be crucial for a model's representation of thermocline mixing, which can ultimately affect the mean ocean state and the variability of both the oceans and atmosphere.

5 DATA AVAILABILITY STATEMENT

All data employed in this study is publicly available. The TAO data is freely downloaded from http://www.pmel.noaa.gov/tao/data_deliv. The gridded Argo salinity data is available at https://www.mmnt.net/db/0/0/ftp.ifremer.fr/ifremer/argo. The surface velocity variance data is available at https://www.aoml.noaa.gov/phod/gdp/mean_velocity.php.

References

Cherian D A, Whitt D B, Holmes R M et al. 2021. Off-Equatorial deep-cycle turbulence forced by tropical instability waves in the equatorial Pacific. *Journal of Physical Oceanography*, **51**(5): 1575-1593, https://doi.org/10.1175/JPO-D-20-0229.1.

Freitag H P, Sawatzky T A, Ronnholm K B et al. 2005. Calibration procedures and instrumental accuracy estimates of next generation ATLAS water temperature and pressure measurements. Silver Spring, MD: United States Department of Commerce, National Oceanic and Atmospheric Administration, Office of Oceanic and Atmospheric Research.

Gregg M C, Peters H, Wesson J C et al. 1985. Intensive measurements of turbulence and shear in the equatorial undercurrent. *Nature*, **318**(6042): 140-144, https://doi.org/10.1038/318140a0.

Inoue R, Lien R C, Moum J N. 2012. Modulation of equatorial turbulence by a tropical instability wave. *Journal of Geophysical Research*: *Oceans*, **117**(C10): C10009, https://doi.org/10.1029/2011JC007767.

Laurindo L C, Mariano A J, Lumpkin R. 2017. An improved near-surface velocity climatology for the global ocean from drifter observations. *Deep Sea Research Part I*: *Oceanographic Research Papers*, **124**: 73-92, https://doi.org/10.1016/j.dsr.2017.04.009.

Lien R C, Caldwell D R, Gregg M C et al. 1995. Turbulence variability at the equator in the central Pacific at the beginning of the 1991-1993 El Niño. *Journal of Geophysical Research*: *Oceans*, **100**(C4): 6881-6898, https://doi.org/10.1029/94JC03312.

Liu C Y, Fang L Y, Köhl A et al. 2019a. The subsurface mode tropical instability waves in the equatorial Pacific Ocean and their impacts on shear and mixing. *Geophysical Research Letters*, **46**(21): 12270-12278, https://doi.org/10.1029/2019GL085123.

Liu C Y, Köhl A, Liu Z Y et al. 2016. Deep-reaching thermocline mixing in the equatorial Pacific cold tongue. *Nature Communications*, **7**: 11576, https://doi.org/10.1038/NCOMMS11576.

Liu C Y, Wang X W, Köhl A et al. 2019b. The northeast-southwest oscillating equatorial mode of the tropical instability wave and its impact on equatorial mixing. *Geophysical Research Letters*, **46**(1): 218-225, https://doi.org/10.1029/2018GL080226.

Liu C Y, Wang X W, Liu Z Y et al. 2020. On the formation of a subsurface weakly sheared laminar layer and an upper thermocline strongly sheared turbulent layer in the eastern equatorial Pacific: interplays of multiple-time-scale equatorial waves. *Journal of Physical Oceanography*, **50**(10): 2907-2930, https://doi.org/10.1175/JPO-D-19-0245.1.

McPhaden M J. 1995. The tropical atmosphere ocean array is completed. *Bulletin of the American Meteorological Society*, **76**(5): 739-744, https://doi.org/10.1175/1520-0477-76.5.739.

Meehl G A, Gent P R, Arblaster J M et al. 2001. Factors that affect the amplitude of El Niño in global coupled climate models. *Climate Dynamics*, **17**(7): 515-526, https://doi.org/10.1007/PL00007929.

Miles J W. 1961. On the stability of heterogeneous shear flows. *Journal of Fluid Mechanics*, **10**(4): 496-508, https://doi.org/10.1017/S0022112061000305.

Moum J N, Caldwell D R. 1985. Local influences on shear-flow turbulence in the equatorial ocean. *Science*, **230**(4723): 315-316, https://doi.org/10.1126/science.230.4723.315.

Moum J N, Hebert D, Paulson C A et al. 1992. Turbulence and internal waves at the equator. Part I: Statistics from towed thermistors and a microstructure profiler. *Journal of Physical Oceanography*, **22**(11): 1330-1345, https://doi.org/10.1175/1520-0485(1992)022<1330:TAIWAT>2.0.CO;2.

Moum J N, Lien R C, Perlin A et al. 2009. Sea surface cooling at the Equator by subsurface mixing in tropical instability waves. *Nature Geoscience*, **2**(11): 761-765, https://doi.org/10.1038/ngeo657.

Moum J N, Nash J D, Smyth W D. 2011. Narrowband oscillations in the upper equatorial ocean. Part I: Interpretation as shear instabilities. *Journal of Physical*

Oceanography, **41**(3): 397-411, https://doi.org/10.1175/2010JPO4450.1.

Moum J N, Perlin A, Nash J D et al. 2013. Seasonal sea surface cooling in the equatorial Pacific cold tongue controlled by ocean mixing. *Nature*, **500**(7460): 64-67, https://doi.org/10.1038/nature12363.

Natarov A, Richards K J. 2019. Enhanced energy dissipation in the equatorial pycnocline by wind-induced internal wave activity. *Journal of Geophysical Research*: *Oceans*, **124**(8): 6200-6217, https://doi.org/10.1029/2019JC015228.

Peters H, Gregg M C, Sanford T B. 1991. Equatorial and off-equatorial fine-scale and large-scale shear variability at 140°W. *Journal of Geophysical Research*: *Oceans*, **96**(C9): 16913-16928, https://doi.org/10.1029/91JC01317.

Plimpton P E, Freitag H P, McPhaden M J. 1997. ADCP velocity errors from pelagic fish schooling around equatorial moorings. *Journal of Atmospheric and Oceanic Technology*, **14**(5): 1212-1223, https://doi.org/10.1175/1520-0426(1997)014<1212:AVEFPF>2.0.CO;2.

Rohr J J, Itsweire E C, Helland K N et al. 1988. Growth and decay of turbulence in a stably stratified shear flow. *Journal of Fluid Mechanics*, **195**: 77-111, https://doi.org/10.1017/S0022112088002332.

Smyth W D, Moum J N. 2000. Length scales of turbulence in stably stratified mixing layers. *Physics of Fluids*, **12**(6): 1327-1342, https://doi.org/10.1063/1.870385.

Smyth W D, Moum J N. 2013. Marginal instability and deep cycle turbulence in the eastern equatorial Pacific Ocean. *Geophysical Research Letters*, **40**(23): 6181-6185, https://doi.org/10.1002/2013GL058403.

Thorpe S A, Liu Z Y. 2009. Marginal instability? *Journal of Physical Oceanography*, **39**(9): 2373-2381, https://doi.org/10.1175/2009JPO4153.1.

Wang W M, McPhaden M J. 1999. The surface-layer heat balance in the equatorial Pacific Ocean. Part I: Mean seasonal cycle. *Journal of Physical Oceanography*, **29**(8): 1812-1831, https://doi.org/10.1175/1520-0485(1999)029<1812:TSLHBI>2.0.CO;2.

Wang W M, McPhaden M J. 2001. What is the mean seasonal cycle of surface heat flux in the equatorial Pacific? *Journal of Geophysical Research*: *Oceans*, **106**(C1): 837-857, https://doi.org/10.1029/1999JC000076.

Warner S J, Moum J N. 2019. Feedback of mixing to ENSO phase change. *Geophysical Research Letters*, **46**(23): 13920-13927, https://doi.org/10.1029/2019GL085415.